COMPACT SRF LINAC FOR HIGH BRILLIANCE INVERSE COMPTON SCATTERING LIGHT SOURCE

K. E. Deitrick*, G. A. Krafft[1], B. Terzič, J. R. Delayen[1],
Center for Accelerator Science, Old Dominion University, Norfolk, VA, 23529, USA
[1]also at Thomas Jefferson National Accelerator Facility, Newport News, VA 23606, USA

Abstract

New designs for compact SRF linacs can produce micron-size electron beams. These can be used for inverse Compton scattering light sources of exceptional flux and brilliance.

INTRODUCTION

Currently, there exist many x-ray techniques which are used in several different fields, including material science, cultural heritage, medicine, national security, and basic research in biology, chemistry, and physics. While a number of light source facilities around the world produce very high quality X-ray beams, there is a significant gap between this performance and the one most X-ray users experience from their laboratory-scale sources.

Increasing research over recent years has been aimed at bridging this gap through compact inverse Compton light sources (ICLSs). One of the significant benefits of this type of source is their production of narrow bandwidth x-ray beams, which is not a feature of most typical small-scale sources, but is required for a number of techniques. In the most general description, the target specifications for these compact ICLS designs has been for high average flux, high average brilliance x-rays - while keeping the requisite electron accelerator compact in size and cost. The design presented here, shown in Fig. 1, has the highest anticipated performance to date among compact Inverse Compton Light Source (ICLS) designs.
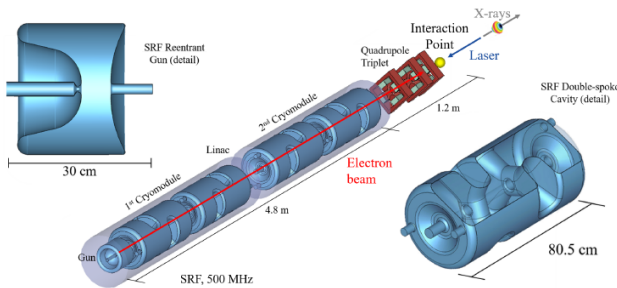

Figure 1: A schematic of the entire design. The first cryomodule contains the gun and two double-spoke cavities, the second contains the last two double-spoke cavities. Three quadrupole magnets follow the linac, before the interaction point. Detailed images of the gun and the double-spoke cavity are shown in the top left and bottom right, respectively.

* kdeit001@odu.edu; deitrick@jlab.org

INVERSE COMPTON SCATTERING

Compton scattering is the process of scattering a photon off of an electron at rest. Inverse Compton scattering (ICS) is the process of scattering a photon off a moving electron, leading the electron losing energy in the process. This collision between electron beam and incident laser occurs at the interaction point (IP).

For this compact ICLS design, we operate in a regime where the Thomson formula is a good approximation - the energy of the incident laser in the beam frame is significantly less than the rest mass of the electron. Consequently, the energy of the x-rays produced in the collision are given by

$$E_x(\Phi, \theta) \approx E_{\text{laser}} \frac{1 - \beta \cos \Phi}{1 - \beta \cos \theta}, \tag{1}$$

where Φ is the angle between the electron beam and scattering laser, θ is the angle between the electron beam and generated x-rays, E_{laser} is the energy of the incident scattering laser, and β is the relativistic factor v_z/c of the electron beam. For a head-on collision, the highest energy x-rays are those scattered in the same direction as the electron beam is traveling; this is the case shown in Fig. 1. The energy of these x-rays is given by $E_x(\Phi = \pi, \theta = 0) \approx \gamma^2(1+\beta)^2 E_{\text{laser}} \approx 4\gamma^2 E_{\text{laser}}$, where γ is the typical relativistic factor for the electron beam and is significantly greater than 1.

The number of scattered x-rays from this collision is given by

$$N_x = \sigma_T \frac{N_e N_{\text{laser}}}{2\pi(\sigma_e^2 + \sigma_{\text{laser}}^2)}, \tag{2}$$

where σ_T is the Thomson cross section, N_e is the number of electrons in the bunch, N_{laser} is the number of photons in the scattering laser, σ_e is the *rms* size of the electron beam, and σ_{laser} is the *rms* size of the laser. The assumption behind this formula and those following is that the distribution of both the electron and laser beams are Gaussian. The number of x-rays within a 0.1% bandwidth at the highest possible x-ray energy is $N_{0.1\%} = 1.5 \times 10^{-3} N_x$, so it follows that the flux into this bandwidth is $\mathcal{F}_{0.1\%} = 1.5 \times 10^{-3} \dot{N}_x$. For high frequency repetitive sources, $\dot{N}_x = f N_x$, where f is the repetition rate.

The spectral brightness or brilliance of an x-ray beam is the density of x-rays in the six-dimensional phase space containing the beam. The general formula for the brilliance of an x-ray beam into a 0.1% bandwidth is

$$\mathcal{B} = \frac{\mathcal{F}_{0.1\%}}{4\pi^2 \sigma_{\gamma,x} \sigma_{\gamma,x'} \sigma_{\gamma,y} \sigma_{\gamma,y'}} \tag{3}$$

where $\sigma_{\gamma,x}$ and $\sigma_{\gamma,y}$ are the *rms* transverse sizes of the x-ray beam and $\sigma_{\gamma,x'}$ and $\sigma_{\gamma,y'}$ are the *rms* transverse angular sizes of the x-ray beam. However, by taking advantage of the analogy to undulator radiation, it is possible to approximate the brilliance of the scattered photons using the parameters of the electron beam at the collision. The standard approximation for a non-diffraction limited beam is $\sigma_{\gamma,x'} \approx \sqrt{\epsilon_x/\beta_x}$, where ϵ_x and β_x are parameters of the electron beam. Taking this approximation into account, Eq. (3) becomes

$$\mathcal{B} = \frac{\mathcal{F}_{0.1\%}}{4\pi^2 \sigma_{\gamma,x}\sqrt{\epsilon_x/\beta_x}\,\sigma_{\gamma,y}\sqrt{\epsilon_y/\beta_y}}. \quad (4)$$

The approximation that the x-ray source size is the size of the electron is typical in the characterization of compact sources. In this approach, $\sigma_{\gamma,x} = \sigma_x = \sqrt{\beta_x\epsilon_x}$, so Eq. (4) becomes

$$\mathcal{B} \approx \frac{\gamma^2 \mathcal{F}_{0.1\%}}{4\pi^2 \epsilon^N_{x,rms}\epsilon^N_{y,rms}}. \quad (5)$$

If instead we take the position that the source size is a convolution of the electron and laser beam sizes, such that

$$\frac{1}{\sigma_\gamma^2} = \frac{1}{\sigma_{laser}^2} + \frac{1}{\sigma_x\sigma_y}. \quad (6)$$

Using this, Eq. (4) becomes

$$\mathcal{B} \approx \frac{\gamma \mathcal{F}_{0.1\%}}{4\pi^2 \sigma_\gamma^2 \sqrt{\epsilon^N_{x,rms}\epsilon^N_{y,rms}/\beta_x\beta_y}}. \quad (7)$$

As the laser spot size becomes increasingly greater than the electron beam spot size, the difference between Eq. (5) and Eq. (7) becomes negligible. However, for the compact source presented here, the spot sizes are roughly equivalent, making Eq. (7) more appropriate. From either brilliance formula, it becomes clear that to maximize brilliance requires maximizing the photon flux, maximizing the electron beam energy, or minimizing the electron beam normalized *rms* transverse emittances [1].

DESIGN CONSIDERATIONS

There are two pieces in an ICLS - a relativistic electron beam and an incident laser. In recent years, laser technology has made significant progress in producing suitable lasers - the details of this advancement are largely out of the scope of this paper. Instead, we assume an ideal scattering laser and focus on the development of a compact linac for a high-flux, high-brilliance ICLS that is compact, relatively affordable, and feasible for non-expert operation.

The desire for a high average flux x-ray beam leads to cw operation and an SRF linac, while cost concerns and operation ease suggest a cryogenics system of atmospheric helium at 4.2 K or above. This temperature necessitates a low-frequency system, in the range of 300 to 500 MHz. In this frequency range, TM$_{010}$ cavities are too large, leading towards the use of spoke cavities in the linac. While a 325 MHz single-spoke cavity has been developed, it was also

Table 1: Desired Electron Beam Parameters at Interaction Point

Parameter	Quantity	Units
Kinetic energy	25	MeV
Bunch charge	10	pC
Repetition rate	100	MHz
Average current	1	mA
Transverse *rms* normalized emittance	0.1	mm mrad
$\beta^*_{x,y}$	5	mm
$\sigma_{x,y}$	3.2	μm
FWHM bunch length	3 (0.9)	psec (mm)
rms energy spread	7.5	keV

deemed too large, leading to the decision of using 500 MHz double-spoke cavities. However, further advancements in SRF technology could lead to reconsidering the geometry and/or frequency choice.

The goal for high flux also leads to a high repetition rate of 100 MHz and a small spot size of 3.2 μm at the IP. This small spot size is made possible by a low bunch charge of 10 pC, which allows for a low transverse normalized *rms* emittance of 0.1 mm mrad and results in an increased brilliance of the x-ray beam. While this emittance is smaller than other reentrant gun designs, the bunch charge makes it attainable. Additionally, this low emittance and low bunch charge is comparable to current high performance normal temperature guns.

An electron beam kinetic energy of 25 MeV and an incident scattering laser energy of 1.24 eV were chosen, leading to the production of x-rays with energies of up to 12 keV. To control energy smearing of the forward flux, the relative beam energy spread needs to be less than 0.03%. At the energy of 25 MeV, this leads to *rms* energy spread of no more than 7.5 keV. To limit the flux reduction due to the hourglass effect, the bunch length at the IP needs to be less than 1 mm. All of the desired electron beam properties at IP are summarized in Table 1.

To evaluate the performance of this electron beam as an x-ray source, we assumed a high-quality, high-power laser. This ideal laser would have a circulating power of 1 MW, a wavelength of 1 μm (1.24 keV), rep rate of 100 MHz, *rms* pulse duration of 2/3 ps, and a spot size of 3.2 μm. Due to the difficulties associated with achieving a 3.2 μm laser spot, we also consider the case of a 12 μm spot laser, while keeping the electron spot size at 3.2 μ. These properties are summarized in Table 2.

Using the properties in Tables 1 and 2 with the formulae presented in the previous section, we can calculate the anticipated properties of the resulting x-ray beam. However, the extremely short Rayleigh range of the laser spot size requires that a reduction factor must be applied. Using the formulae given in [2], we anticipate a reduction of 85% and 26% for the 3.2 and 12 μm laser spot sizes, respectively.

Table 2: Laser Parameters at Interaction Point

Parameter	Quantity	Units
Wavelength	1 (1.24)	μm (eV)
Circulating power	1	MW
N_γ, Number of photons/bunch	5×10^{16}	
Spot size (*rms*)	3.2, 12	μm
Repetition rate	100	MHz
rms pulse duration	2/3	ps

The anticipated x-ray performance is given in Table 3; for both laser spot sizes, the top energy is 12 keV, the flux is on the order of 10^{13} ph/s, and the average brilliance is on the order of 10^{14} ph/(s mm^2 mrad^2 0.1%BW). The use of a non-diffracting laser beam, such as an Airy or Bessel beam, should lead to a smaller reduction, though it is currently unclear if the use of such a beam would negate or only ameliorate the reduction effect.

ACCELERATING SECTION

SRF Reentrant Gun and Emittance Compensation

We chose to use an SRF reentrant gun, a concept originally proposed in the early 1990s. A few other SRF reentrant guns do exist, none which operate near a 10 pC bunch charge - consequently, none match the emittance goals of this accelerator. However, there do exist high performing normal temperature guns which closely match our desired performance, particularly the Cornell DC gun [3] and the normal conducting rf gun at APEX [4]. Our final gun geometry design is shown at the top left in Fig. 1. The bunch exits the gun with a kinetic energy of 1.5 MeV and a transverse normalized *rms* emittance, $\epsilon^N_{(x,y),\text{rms}}$, of 0.2 mm mrad. While larger than our desired emittance at IP, $\epsilon^N_{(x,y),\text{rms}}$ decreases before exiting the linac due to emittance compensation - the manipulation of a beam's transverse phase space to decrease the projected emittance.

The most critical and challenging electron beam parameter is the $\epsilon^N_{(x,y),\text{rms}}$ at the IP, which must be achieved by emittance compensation. Frequently, emittance compensation is achieved by placing a solenoid following the gun. In this concept, emittance compensation is performed through rf focusing, altering the geometry of the reentrant gun to produce the necessary fields to compensate for the space charge fields of the bunch.

To refine the gun geometry appropriately, the shape was parameterized, shown in Fig. 2, the electromagnetic (EM) fields were calculated using Superfish [5] for the gun and CST Microwave Studio [6] for the double-spoke cavity, and the initial distribution was tracked to the exit of the linac using IMPACT-T [7]. The initial distribution was assumed to be a radially uniform distribution of 1 mm radius, a plateau longitudinal distribution of 4.5 ps, and no initial emittance or energy spread. The main focus was on parameters closest

to the cathode, where the energy of the bunch is lowest and the effect of space charge most significant.
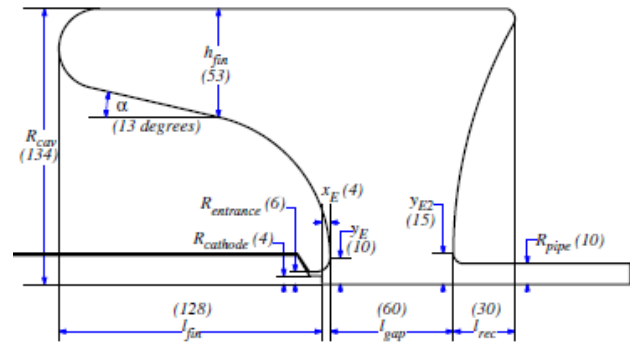

Figure 2: Diagram of gun geometry with parameters and quantities. Quantities are rounded to the nearest millimeter and given in millimeters, except where explicitly indicated.

To demonstrate the effectiveness of this emittance compensation, two horizontal normalized phase spaces are shown in Fig. 3. The normalized phase spaces are shown at the exit of the gun on the left and the exit of the linac on the right, with the particles color-coded according to their longitudinal position within the bunch. Exiting the gun, it is clear to see that the emittance slices along the bunch length are not well-aligned. However, when the bunch exits the linac, these longitudinal slices are better aligned, leading to a significant reduction in projected normalized *rms* emittance.
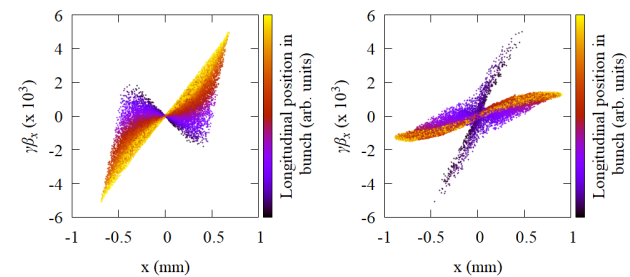

Figure 3: Normalized transverse phase spaces exiting the gun (left) and the linac (right), with the longitudinal position of the particle within the bunch indicated by color. The emittance slices along the bunch length rotate to align better, for a decrease in projected normalized *rms* emittance.

Linac

The linac consists of four double-spoke cavities, shown in detail at the bottom right of Fig. 1, designed by Christopher Hopper during his ODU PhD research [8]. For the emittance compensation to be most effective, the gun and first linac cavity must be placed within the same cryomodule. The double-spoke cavities have a "quadrupole-like" focusing effect on the beam. Consequently, to achieve a relatively round beam at exiting the linac, the center two cavities are rotated so that the beam is focused in both transverse planes.

Table 3: Desired Light Source Parameters. Flux and brilliance reported for top x-ray energy, reduced for lower energies

Parameter	Laser spot (µm)		Units
	3.2	12	
X-ray energy	1.2 - 12	1.2 - 12	keV
Photons/bunch	2.4×10^5	1.6×10^5	
Flux	2.4×10^{13}	1.6×10^{13}	ph/s
Average brilliance	4.4×10^{14}	1.6×10^{14}	ph/(s mm^2 mrad^2 0.1%BW)

Table 4: Select Properties of the Electron Beam Parameters, both Desired and Achieved, at the IP.

Parameter	Desired	Achieved	Units
β_x^*	5	5.4	mm
β_y^*	5	5.4	mm
$\epsilon_{rms,x}^N$	0.1	0.1	mm mrad
$\epsilon_{rms,y}^N$	0.1	0.13	mm mrad
σ_x	3.2	3.4	µm
σ_y	3.2	3.8	µm
> 76% longitudinal distribution	3	3	ps
rms energy spread	7.5	3.4	keV

At the end of the linac, the bunch exits with a kinetic energy of 25 MeV, *rms* transverse sizes less than 0.4 mm, transverse normalized *rms* emittances of 0.1 mm mrad (horizontal) and 0.13 mm mrad, a bunch length of 0.67 mm, and and *rms* energy spread of 3.4 keV.

FINAL FOCUSING

Final focusing is achieved using a quadrupole triplet; simulations were performed using `elegant` [9]. Table 4 compares the target goals of the electron beam and the simulated beam parameters, which are quite close in all parameters. The longitudinal length of the beam containing more than 76% of the beam is quoted instead of the *rms* bunch length because the beam does not have a Gaussian distribution. The beam spot and transverse phase spaces at the IP are shown in Fig. 4. The transverse distributions of the beam at IP is shown in Fig. 5, compared with the distribution of a Gaussian distribution with the same *rms* value. It is clear that the transverse beam distribution is significantly non-Gaussian.
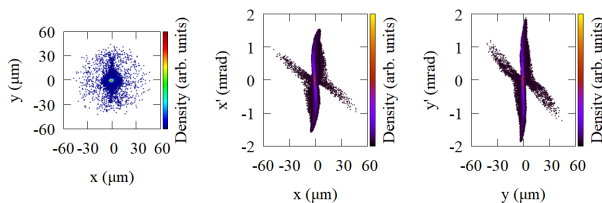

Figure 4: Beam spot (top left), longitudinal phase space (top right), horizontal phase space (bottom left), and vertical phase space (bottom right) of the electron bunch at the IP.
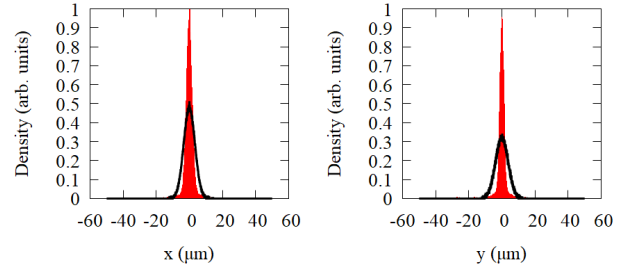

Figure 5: The horizontal (left) and vertical (right) distribution of the start-to-end simulated beam at the IP (red) and a Gaussian distribution with the same *rms* values (black).

X-RAY PERFORMANCE

To evaluate the success of this design, it is not enough to simply compare the electron beam parameters; the anticipated x-ray parameters must be determined. However, Fig. 5 has clearly demonstrated the non-Gaussian distribution of the beam, calling into question the validity of using the formulae presented previously. Improved codes for Compton simulation (ɪᴄᴄꜱ) [10] allows for the calculation of x-ray spectra for an arbitrary electron distribution. Using ɪᴄᴄꜱ, the spectra of the x-ray beam was calculated for both 3.2 and 12 µm, shown in Fig. 6. Using the pin-hole brilliance formula

$$\mathcal{B}_p = \lim_{\theta_a \to 0} \frac{\mathcal{S}_{0.1\%}}{2\pi^2 \sigma_e^2 \theta_a^2}, \qquad (8)$$

where θ_a is the aperture, it is possible to calculate the anticipated brilliance, given in Table 5. Also listed are the average flux and average brilliance, both anticipated and desired. Taken together, several things become clear. First, anticipated flux and brilliance using the Gaussian model for both spot sizes is comparable with the original goals. Second, the anticipated average brilliance is almost the same whether calculated using the Gaussian model or ɪᴄᴄꜱ for the 12 µm case. Finally, the fact that ɪᴄᴄꜱ calculates a much higher brilliance than using the Gaussian model is reasonable, but not physical - the model used in ɪᴄᴄꜱ assumes that every electron sees the same scattering potential. While this is a valid assumption for laser spots much larger than the electron beam szie, it loses validity and leads to overestimation as the sizes become comparable. Overall, however, the anticipated x-ray properties are quite close to the high-flux, high-brilliance source that was the original goal.

Table 5: X-ray performance of the designs attained by numerical simulation with an aperture of $1/40\gamma$ (top) and by formulae from Gaussian model (middle), compared to original design goals (bottom). Suggested aperture for brilliance calculation only.

| Parameter	Laser Spot (μm)		Units
	3.2	12	
X-ray energy	12.3	12.3	keV
$N_{0.1\%}$	1230	92.4	ph/0.1%BW
$\mathcal{S}_{0.1\%}$	1.23×10^{11}	9.24×10^{9}	ph/(s 0.1%BW)
Average brilliance, from ICCS	*7.2×10^{14}	1.18×10^{14}	ph/(s mm^2 mrad^2 0.1%BW)
Average flux, Gaussian model	2.2×10^{13}	1.6×10^{13}	ph/s
Average brilliance, Gaussian model	3.4×10^{14}	1.2×10^{14}	ph/(s mm^2 mrad^2 0.1%BW)
Desired average flux	2.4×10^{13}	1.6×10^{13}	ph/s
Desired average brilliance	4.4×10^{14}	1.6×10^{14}	ph/(s mm^2 mrad^2 0.1%BW)
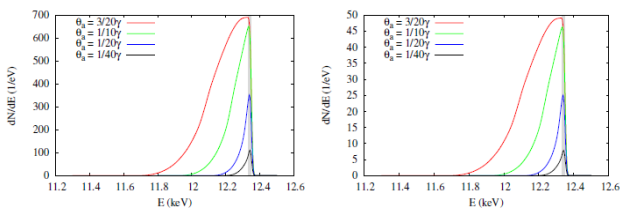
Figure 6: Number spectra for different apertures generated using 4,000 particles for a 3.2 μm laser spot size (left) and a 12 μm laser spot size (right). Grey box indicates 0.1% bandwidth. Suggested apertures for brilliance calculation only.

CONCLUSION

The design concept presented is the highest average brilliance x-ray beam currently proposed by any compact Compton source. While the current parameters are for 12 keV x-rays, placing additional cryomodules after the existing linac can increase the energy of the electron beam, resulting in x-rays with higher energies and a wider range of applications. The high brilliance of this source is achieved through a number of factors, particularly a superconducting drive linac operating cw at 4 K and an electron beam with a low emittance and small spot size at the IP, made possible by a low bunch charge and emittance compensation through rf focusing, instead of the more typical solenoid. With the proper R&D, this promises an exceptional x-ray source; further details are available in [1].

ACKNOWLEDGEMENTS

REFERENCES

[1] K. E. Deitrick, G. A. Krafft, B. Terzić, and J. R. Delayen, *Phys. Rev. Accel. Beams*, vol. 21, p. 080703, 2018.

[2] M. A. Furman, in *Proc. PAC'91*, San Francisco, CA, USA, May 1991, pp. 422-424.

[3] C. Gulliford *et al.*, *Phys. Rev. ST Accel. Beams*, vol. 16, p. 073401, 2013.

[4] F. Sannibale *et al.*, *Phys. Rev. ST Accel. Beams*, vol. 15, p. 103501, 2012.

[5] "Poisson Superfish," http://laacg.lanl.gov/laacg/services/download_sf.phtml, 2012.

[6] "Computer simulation technology website," http://www.cst.com.

[7] J. Qiang, S. Lidia, R. D. Ryne, and C. Limborg-Deprey, *Phys. Rev. ST Accel. Beams*, vol. 9, p. 044204, 2006.

[8] C. S. Hopper, Ph.D. thesis, Old Dominion University, 2015.

[9] M. Borland, Advanced Photon Source LS-287, 2000.

[10] N. Ranjan, B. Terzić, G. A. Krafft, V. Petrillo, I. Drebot, and L. Serafini, *Phys. Rev. Accel. Beams*, vol. 21, p. 030701, 2018.